



HIRISE: a ground-based high-resolution imaging spectrograph using echelle grating for measuring daytime airglow/auroral emissions

D. Pallamraju *, J. Baumgardner, S. Chakrabarti

Center for Space Physics, Boston University, 725 Commonwealth Avenue, Boston, MA 02215, USA

Abstract

We discuss a new optical technique for measuring daytime optical emissions. We elucidate the method of analysis for retrieving the daytime airglow and auroral emissions using this instrument and explain the procedure used to account for the Ring effect contribution. Finally, we show sample results of thermospheric oxygen dayglow emissions obtained by this instrument. © 2002 Elsevier Science Ltd. All rights reserved.

PACS: 94.10.Rk; 94.80.+g; 95.75.Fg

Keywords: O I 630.0 nm dayglow; Daytime aurora; Ring effect; Echelle spectrograph; Instruments and techniques

1. Introduction

The Earth's upper atmosphere responds to the energy inputs from above (solar radiation, particle precipitation, etc.) and from below (gravity waves). Out of the various channels for loss of energy in this region, the loss via airglow emissions is significant and needs to be understood to eventually take into account the net energy budget of the upper atmosphere (Roble, 1995). Optical emissions from atomic and molecular constituents of the earth's atmosphere yield useful information on the behavior of the altitude regions of their origin (such as the neutral temperature, winds, gravity waves, etc.). Numerous measurements of the nighttime airglow (nightglow) have been carried out from both space-borne and ground-based platforms for several decades now. Nighttime measurements of integrated airglow emission rates at various wavelengths have been used to infer the thermospheric behavior under varying geophysical conditions from different latitudes. In contrast, there have

been very few ground-based optical measurements during daytime due to the presence of strong solar background continuum which is several orders of magnitude higher in brightness when compared to the daytime airglow (dayglow) emission contribution. There have been only a few satellite-based measurements of visible airglow emissions during daytime (Hays et al., 1978; Shepherd et al., 1993). Although the satellite measurements provide a very good spatial coverage, they lack information on the temporal evolution of the emissions at a given location. Furthermore, due to the ground albedo, they are limited in their zenith angle coverage as well. Ground-based measurements, on the other hand, complement satellite-based measurements by providing excellent information on the time-evolution and complete zenith angle coverage of the emission intensities. Hence, there has always been a need for newer techniques for ground-based measurements of dayglow emissions. Earlier, different techniques, such as, spectral scanning polarimeter (Noxon and Goody, 1962), poly-etalon Fabry–Perot interferometers (e.g., Bens et al., 1965; Barmore, 1977; Cocks et al., 1980; Greet et al., 1989; Rees et al., 2000) and a single Fabry–Perot etalon in conjunction with a novel mask system (Narayanan et al., 1989; Sridharan et al., 1993, 1998) have been employed to measure the dayglow emission rates. Here

* Corresponding author. Tel.: +1-617-353-5990; fax: +1-617-353-6463.

E-mail addresses: dprraju@bu.edu (D. Pallamraju), jeff@bu-ast.bu.edu (J. Baumgardner), supc@bu.edu (S. Chakrabarti).

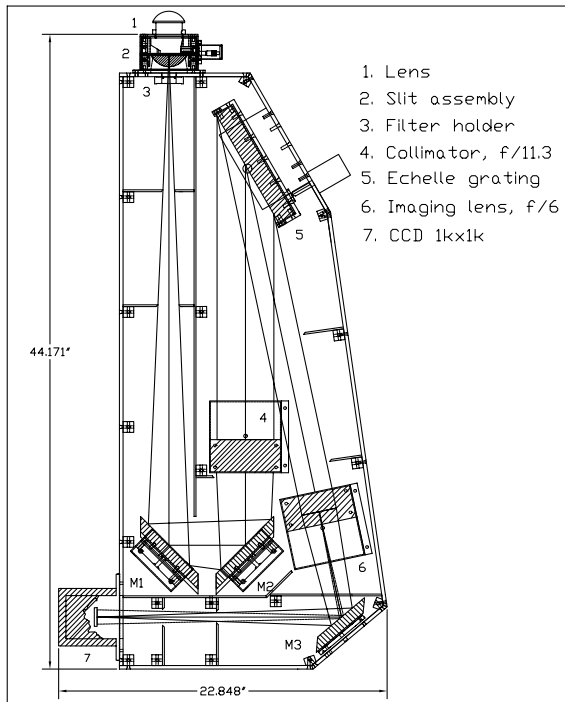


Fig. 1. Schematic of HIRISE showing various components and the layout of the optical paths in the system. M1, M2 and M3 are the folding mirrors.

we present a new technique developed at Boston University, which employs an echelle grating spectrometer for measuring daytime airglow emissions. This instrument, called the high-resolution imaging spectrograph using echelle grating (HIRISE), is a daytime (high-resolution) variant of the HiTIES (high throughput) instrument (Chakrabarti, 1998; Chakrabarti et al., 2001). HIRISE is capable of obtaining comprehensive, high-resolution spectra at multiple wavelengths simultaneously. In this paper we present some of the field tests carried out by HIRISE. These results display its enormous potential and demonstrate its capability for measuring the daytime airglow emissions. Here, we also describe the method of extraction of dayglow emissions buried in the strong daytime background continuum. A sample of actual measurements of the integrated emission rates of O I 6300 Å dayglow obtained using HIRISE is also presented. Use of HIRISE resulted in resolving the controversies of Ring effect variability (Pallamraju et al., 2000) and in obtaining the first observations of a daytime auroral arc in O I 6300 Å emissions as verified by the incoherent scatter radar from Sondrestromfjord in Greenland (Pallamraju et al., 2001).

2. HIRISE

HIRISE (Fig. 1) is a long slit echelle spectrograph that uses an interference filter behind the slit for order separation,

an echelle grating as the dispersing element and a 1024×1024 pixels CCD detector to record a high-resolution spectrum. This section briefly describes the principle of operation of HIRISE.

An objective lens in front of the slit determines the field-of-view (fov) of HIRISE. The light gathered by this lens falls on the slit. All of the light that passes through the slit is made to fall onto the collimator by placing a field lens behind it. This lens also images the front objective onto the collimator. We place an interference filter (of about 100 \AA FWHM) behind the field lens to allow light of only a narrow spectral region to pass through. This spectrally selected light is collimated by an $f/11$ apochromat lens and is subsequently allowed to fall on the grating.

The key element of HIRISE is the grating. The grating equation is given as

$$m\lambda = d(\sin \alpha + \sin \beta),$$

where, m is the order of diffraction, λ is the wavelength, d is the groove spacing, and α and β are the incident and diffraction angles, respectively.

For a fixed angle of incidence we can find the angular dispersion by differentiating the grating equation

$$d\beta/d\lambda = m/(d \cos \beta).$$

From the above equation it can be seen that if the grating is used in low diffraction order, $m = 1$ or 2 , then high angular dispersion is obtained only with a finely ruled grating, hence small d . On the other hand, it is also possible to obtain large angular dispersion with a coarsely ruled grating, if the diffraction order is sufficiently high. Gratings specifically designed for use at large values of m , and with large angles α and β , are called *echelles*. These are a special class of high blaze-angle gratings which have higher resolution and dispersion and smaller free spectral range compared to ordinary gratings. The grating used in HIRISE has a ruling density of $98.6 \text{ lines mm}^{-1}$; a blaze angle of 63.5° and is operated in high diffraction orders (typically between 25–45).

The diffracted rays from the grating are made to focus onto a CCD detector by an $f/6$ (another apochromat) camera lens. By using this lower focal ratio lens as compared to the collimator, the image from the 40 mm long slit is reduced in size to fit onto a 24 mm wide (SITE) CCD chip. M1, M2 and M3 labeled in Fig. 1 are flat mirrors used to fold the bundle of rays. The orientation of the CCD is arranged so that the columns contain information along the dispersion direction and the rows contain information along the slit. The CCD is usually cooled to at least -35°C and has a dark signal of $0.1 \text{ electrons s}^{-1} \text{ pixel}^{-1}$ and a read noise of 6 electrons RMS. The detector has a quantum efficiency of approximately 80% in a wide spectral range (3900–8000 Å) and its pixel size is 0.024 mm, which is about three times larger than the diffraction limit of the optics (0.0092 mm) at 6500 Å. Hence, the pixel size limits the spectral resolution

Table 1
Characteristics of HIRISE

Slit length	40 mm	
Slit width	0.040–3.0 mm	
Throughput ($A\Omega$)	$3.1229 \times 10^{-4} \text{ cm}^2$	
Collimator	$f = 1130 \text{ mm}$	($F/11$) apochromat
Grating	$98.6 \text{ lines mm}^{-1}$, 63.5° blaze angle echelle	$100 \text{ mm} \times 200 \text{ mm}$
Angle between α and β	12°	
Camera lens	$f = 600 \text{ mm}$	($F/6$) apochromat
Estimated Optical Transmission τ	0.16875	
		Quantum eff. $q(\lambda): 0.8e^- \text{ ph}^{-1}$ λ range: $3900\text{--}8000 \text{ \AA}$ Dark signal: $0.1e^- \text{ s}^{-1} \text{ pixel}^{-1}$ Read noise: $6e^- \text{ RMS}$ Gain, g : $2.656e^- \text{ DN}^{-1}$ Pixel size: 0.024 mm
Detector	Thinned 1024×1024 pixels SITE CCD	
No. of rows (n_{rows})	110 for 8 pixel binning along the slit	
Dispersion d	$0.04 \text{ \AA pixel}^{-1}$	at 5893 \AA
Resolution	0.12 \AA	at 5893 \AA

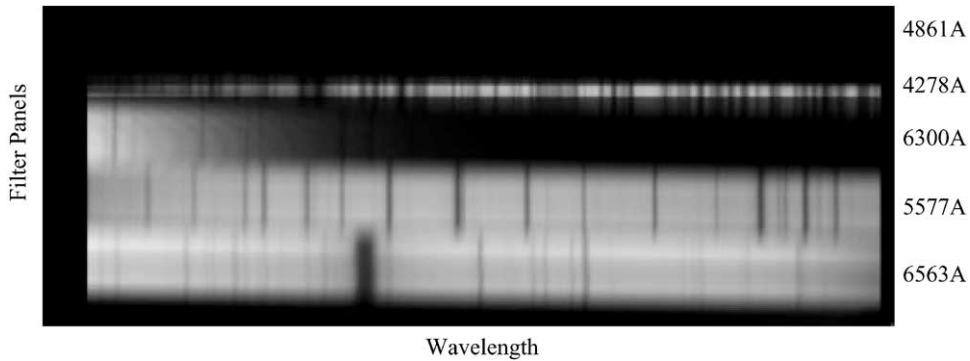


Fig. 2. Multi-spectral image obtained by HIRISE. The five-filter panel used here consists of filters centered around 4861, 4278, 6300, 5577 and 6563 Å. Notice that no light is allowed through the 4861 Å filter and only a part of light is allowed through the 6300 Å filter for this particular diffraction angle. Spectral lines from the rest of the filters can be seen in this figure. Using this spectral image we estimated the resolution at 4278, 5577, and 6563 Å to be 0.07, 0.1 and 0.12 Å, respectively.

achieved by HIRISE. The salient features of HIRISE are summarized in Table 1.

When a grating is operated in higher orders (> 1) there would be various wavelengths (from different orders) in the same diffraction angle range. We can simultaneously obtain spectra from multiple wavelengths by placing a mosaic of filters (multiple interference filters arranged one next to other) perpendicular to the slit orientation. In such an arrangement, owing to the imaging property of HIRISE, the image formed on the CCD consists of segments of spectral information corresponding to the filter array placed in the front-end of the instrument as shown in Fig. 2. An array of 5 filters was used to obtain this image whose spectral bandpass were centered at 4861 (H_β), 4278, 6300, 5577 and 6563 Å (H_α). From this spectral image we estimated the effective resolution achieved by HIRISE to be 0.07, 0.1 and 0.12 Å at 4278, 5577 and 6563 Å, respectively. However, in this arrangement different filters map the sky at different

spatial locations, the extent being dependent on the focal length of the objective lens. Note that different wavelength coverage could be obtained for different sets of α and β . Therefore, to obtain 6300 Å dayglow emission, we could select appropriate α and β to allow the light from the 6300 Å panel to fall on the center of the CCD chip. In actual OI 6300 Å dayglow measurements, we replace the mosaic filter with one (6300 Å) filter to take advantage of all the available area on the CCD chip.

3. Dayglow emission extraction

Airglow/auroral emissions during daytime are obtained by comparing the blue-sky spectrum with the solar spectrum, obtained by HIRISE. The blue-sky spectrum is different from the solar spectrum in terms of atmospheric emissions, atmospheric scattering (Ring effect), and the

depth of the telluric absorption lines. (Telluric absorptions occur due to the absorption of sunlight by the Earth's atmospheric gases as opposed to Fraunhofer absorptions, which are due to the gases in Sun's atmosphere.) Note that the solar and the sky spectra obtained by any instrument are not the 'true' spectra but are a result of convolution of the 'true' spectrum with the instrument function. We are able to scale and compare these two spectra as they are obtained by the same instrument with the same instrumental parameters. The contribution of thermospheric dayglow emission in the solar spectrum is inconsequential as it is very weak compared to the bright solar disk. Hence, the difference between the blue-sky and the scaled solar spectra yields information on contributions due to atmospheric scattering and dayglow emissions.

3.1. The Ring effect

Compared to the solar spectrum the blue-sky spectrum is 'filled-in' at the center of Fraunhofer absorption regions. This feature, called the *Ring effect* (Grainger and Ring, 1962), is believed to be due primarily to Rotational Raman scattering from the atmospheric gas molecules. This effect is also seen in the spectra of various planets in addition to the Earth (Cochran et al., 1981 and references therein). It is important to estimate this contribution as many atmospheric dayglow emissions occur near the Fraunhofer absorption lines. If the data analysis procedure does not properly account for the Ring effect, the dayglow emissions will be overestimated. Different observational and analysis methods use different means to take the Ring effect into account (see for e.g., Tepley et al., 1981; Swift et al., 1990; Conde et al., 1992; Fish and Jones 1995; Pallam Raju et al., 1996). Comprehensive measurements of the Ring effect carried out at various wavelengths simultaneously by HIRISE resulted in resolving the existing controversies in its variability with solar zenith angle and wavelength by bringing out the true dependence of the Ring effect (Pallamraju et al., 2000). It has been shown that the fractional Ring effect depends primarily on the Fraunhofer absorption line strength (normalized depth \times half-width); for a given line strength however, it decreases with wavelength (Pallamraju et al., 2000). Hence, in estimating the intensities of dayglow emissions that emanate in a Fraunhofer absorption region, care should be taken in accounting for the Ring effect contribution at that region by considering the Ring effect contribution from an absorption region that is spectrally *close* to and *similar* in absorption line strength to the Fraunhofer absorption region at the emission wavelength.

4. The O I 6300 Å daytime airglow/aurora

So far, HIRISE has been used primarily to measure the thermospheric emission at 6300.3 Å, which is strongest of the daytime emissions (Bates and Dalgarno, 1954). The

spectral image obtained using a 6300 Å filter would look similar to the image shown in Fig. 2 except that there would be spectral lines of only one wavelength range (i.e. only one of the five panels, described earlier) all along the slit orientation. Due to the imaging property of this spectrograph, the y -axis (whose orientation is along the length of the slit) of such an image corresponds to the light obtained from different regions in the sky. We obtain information on the thermospheric dayglow emission at 6300 Å when we compare this image with the solar spectral image obtained by the same instrument. With a knowledge of, or assumption about, the altitude of the emission one can map different rows on the image to latitudes/longitudes in space (depending on the orientation of the slit either along north–south or east–west direction). We divide the image along the y -axis into different groups, each of several rows. Then, the data numbers (DN) (counts) of each row in a group are averaged to obtain a better signal-to-noise ratio (SNR). Such spectra from different groups represent the contribution from different spatial regions on the sky.

A representative plot (shown in Fig. 3a) obtained from a blue-sky image is compared to the reference solar spectrum to match the continuum regions on either side of the emission wavelength of interest by a least-squares technique. This 'reference solar spectrum' is derived from an average of several (usually many tens of) solar images obtained by HIRISE to improve the SNR of the measurement. In panel 3b the solid line shows the solar spectrum in the wavelength region (6299.8–6301.2 Å) of interest. The dashed line shows the sky spectrum scaled at the continuum in wavelength region 1 (6299.85–6300.05 Å). Notice that it does not match very well in region 2 (6300.85–6301.05 Å) which is the continuum region on the other side of the dayglow emission. The dotted line shows the least-squares matching performed at the continuum region 2, and it can be seen that this does not match well with the continuum at region 1. The uncertainty in a measured value is described by Poisson distribution. Hence, if x counts are obtained during an observation, the uncertainty in this measurement would be $\pm\sqrt{x}$ as shown in panels 3b and 3c. Furthermore, as in the present case, when two measured values, say x and y are subtracted, their uncertainty is given by the square root of their sum ($\sqrt{(x+y)}$) as shown in panel 3d. Hence, the SNR is given by $((x-y)/\sqrt{(x+y)})$. The SNR improves with larger time integration or averaging many spectral images. It can be seen that the mismatch between the continuum levels in Fig. 3b is more than the $\pm 1\sigma$ error bar when only one continuum region is used for scaling. Hence, in practice, we use the scaling factors obtained by individually matching both these regions, and calculate them as a function of wavelength. These scaling factors are multiplied with the corresponding solar spectrum values to obtain a better match to the blue-sky spectrum, as can be seen in Fig. 3c. Here, the dash-dot line shows the blue-sky spectrum and the solid line shows the solar spectrum scaled using the procedure described above. The difference between such spectra (shown

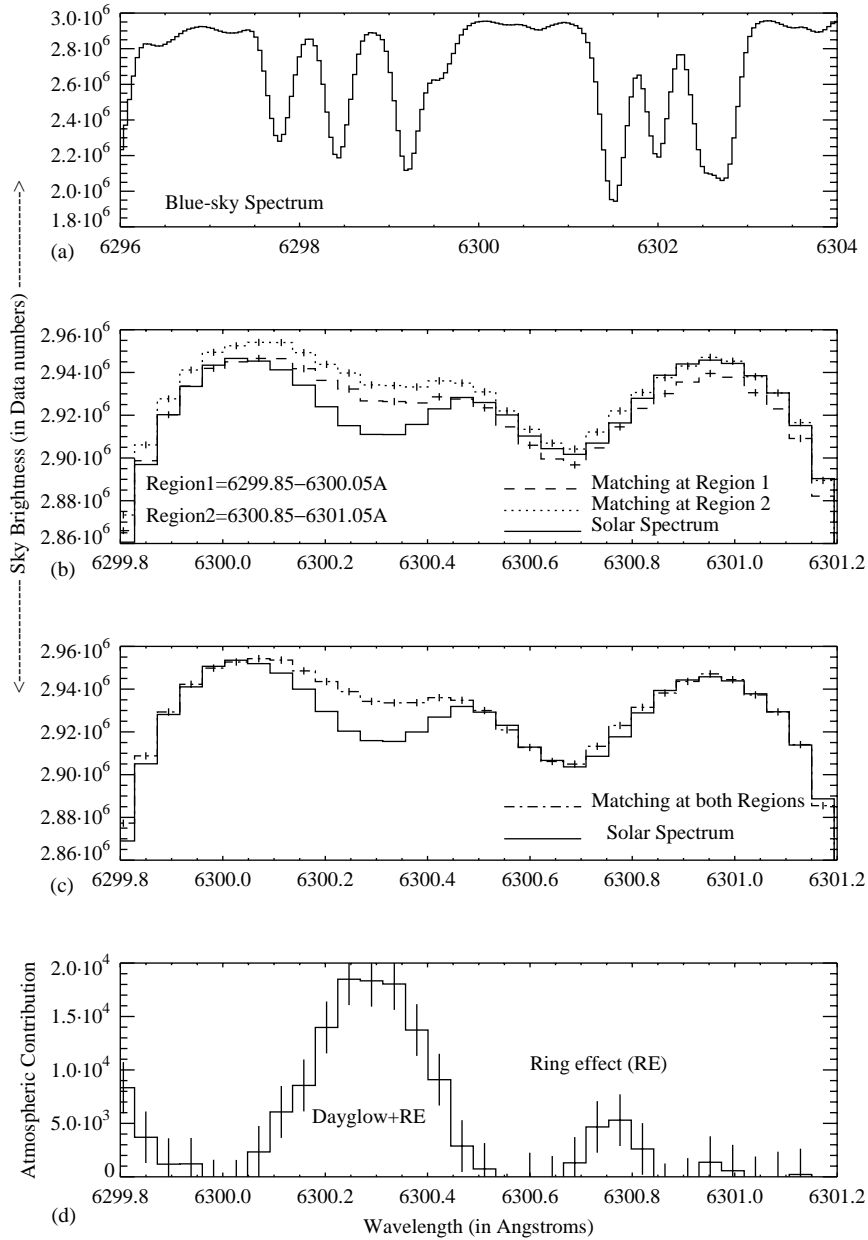


Fig. 3. The intricacies involved in the data analysis procedure are depicted. Panel (a) shows the blue-sky spectrum obtained using a 6300 Å filter (FWHM 100 Å). This spectra shows various Fraunhofer absorption lines around 6300 Å region. Panel (b) shows the need for matching the continuum regions on either side of the emission wavelength (see text for details). (c) Scaled solar and blue-sky spectra after the least-squares matching at the continuum regions on either side of the emission line of interest at 6300.3 Å. (d) Atmospheric contribution around the 6300 Å region, obtained by subtracting the solar spectrum from the blue-sky spectrum shown in the above panel. Error ($\pm 1\sigma$) bars are also shown.

in panel 3c) results in the atmospheric contribution as can be seen in Fig. 3d. One can clearly notice the dayglow and the Ring effect contributions in this panel along with $\pm 1\sigma$ error bars. The area under the curve at 6300.7 Å is calculated and subtracted from the curve at 6300.3 Å to account

for the Ring effect contribution at 6300.3 Å region. The remaining amount yields the O I 6300.3 Å dayglow emission contribution. The only assumption here is that the Ring effect contribution at these two Fraunhofer absorption regions is identical since they are close to one another in wavelength

space and are of nearly the same line strength. Analysis of the kind explained above is repeated for different times on a given day to obtain a diurnal behavior of the O I 6300.3 Å dayglow emissions.

5. Emission intensity estimation

One can make an approximate estimate of emission intensities with a knowledge of the parameters of various components used in the instrument. For a brightness B of the source in Rayleighs (R), the number of photons passing through the instrument is $N = BS_t$, where t is the integration time, S is the sensitivity of the instrument expressed in (data numbers) $\text{DN s}^{-1} \text{R}^{-1}$. At any given pixel, the sensitivity per Angstrom can be written as

$$S_{\text{pix}} = 10^6 / 4\pi Q(\lambda) \tau A \Omega d / n_{\text{rows}},$$

where, $Q(\lambda)$ is the overall efficiency of the CCD (quantum efficiency $q(\lambda)/\text{gain } g$), τ is the optical efficiency of the instrument, A is the area of the slit, Ω is the solid angle of the sky that the slit ‘sees’, d is the dispersion in Å pixel^{-1} and n_{rows} are the number of rows that have been co-added in the spatial dimension. From the values given in Table 1 it can be seen that the sensitivity of HIRISE is

$$S_{\text{pix}} = 4.6 \times 10^{-4} (\text{DN Å R}^{-1} \text{s}^{-1}).$$

Therefore, dividing the data numbers obtained by the CCD with the sensitivity, one can make a *theoretical estimate* of the absolute emissions.

In addition, one can make an empirical estimate of the absolute intensities by using a lamp of known intensity at the wavelength of interest. We used a C-14 radioactive source, whose intensity with wavelength is precisely known, to calibrate an incandescent lamp of higher intensity. We treated this (secondary) lamp as the ‘standard lamp source’ to carry out an *empirical estimate* of the absolute intensities. The procedure followed in this method is to divide the blue-sky images by an averaged standard source image to obtain ‘flat-fielded’ blue-sky spectral images. The resulting data numbers obtained after following the analysis procedure described in Section 4 are multiplied by the intensity of the source lamp to yield emissions in Rayleighs. This method is preferable to the theoretical estimation method described above, as in that method it is not possible to know the ‘exact’ values of various parameters of the components used in the instrument. On the other hand, in the empirical estimation method the effect due to various optical components are inherently taken into account as their response is expected to be the same for both the standard lamp and blue sky.

Fig. 4 shows a sample data obtained from Boston on May 14, 2000. The measurements are shown as ‘+’ marks and are calibrated using the empirical method described above. A 11-point running average for these data points is also shown (dashed line). The absolute emission rates

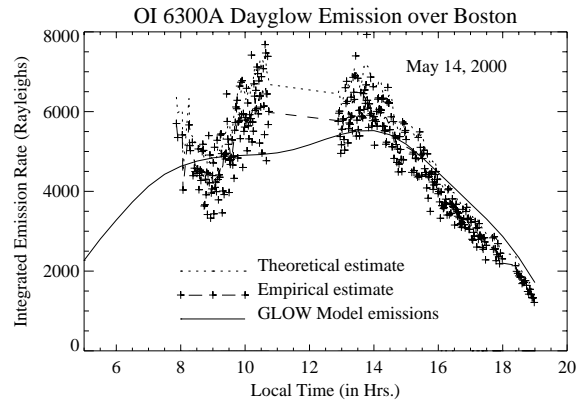


Fig. 4. Sample data showing the O I 6300 Å column-integrated dayglow emission rate obtained over Boston on May 14, 2000. Absolute emissions obtained using theoretical and empirical methods are depicted (see text for details). The solid line shows the model emissions using the GLOW model. The good agreement between the measurements and model demonstrates the capability of HIRISE.

obtained by the theoretical method described above are also shown as the dotted line (11-point running average). It is encouraging to see that there is a good agreement between both the methods of absolute emission rate estimation (with approximately 10–15% discrepancy in the emissions). The primary contributors to the O I 6300 Å emission are: (a) photoelectron impact, (b) photodissociation and (c) dissociative recombination. Using the geophysical conditions for that day we estimated the integrated volume emission rates using the GLOW model (Solomon and Abreu, 1989), the result of which is depicted by the solid line in Fig. 4. The close similarity between the measured and model emissions demonstrates the potential of HIRISE and gives credence to the measurements carried out by HIRISE.

6. Summary

We have described a new high-resolution imaging spectrograph using an echelle grating (HIRISE) that we built at Boston University. Using the laboratory and field measurements we have also demonstrated its capabilities for aeronomy applications. We have also shown a sample data obtained from Boston which show good agreement with model estimates.

Acknowledgements

We thank Dr. Stanley Solomon for providing the GLOW model. This work is supported by the NSF grants ATM-9601846, ATM-0077678 and USRA Student Explorer Demonstration Initiative (STEDI) grant 1500-05.

References

- Barmore, F.E., 1977. High resolution observations of the 6300 Å oxygen line in the day airglow. *Planetary and Space Science* 25, 185–191.
- Bates, D.R., Dalgarno, A., 1954. Theoretical considerations regarding the dayglow. *Journal of Atmospheric and Terrestrial Physics* 5, 329–344.
- Bens, A.R., Cogger, L.L., Shepherd, G.G., 1965. Upper atmospheric temperatures from Doppler line widths-III. Observations of the O I dayglow emission at 6300 Å. *Planetary and Space Science* 13, 551–563.
- Chakrabarti, S., 1998. Ground-based spectroscopic studies of sunlit airglow and aurora. *Journal of Atmospheric and Solar-Terrestrial Physics* 60, 1403–1423.
- Chakrabarti, S., Pallamraju, D., Baumgardner, J., Vaillancourt, J., 2001. HiTIES: a high throughput imaging echelle spectrograph for ground-based visible airglow and auroral studies. *Journal of Geophysical Research* 106, 30,337–30,348.
- Cochran, W.D., Trafton, L., Macy, W., Woodman, J.H., 1981. Raman scattering in the Jovian atmosphere. *Astrophysical Journal* 247, 734–740.
- Cocks, T.D., Creighton, D.F., Jacka, F., 1980. Application of a dual Fabry–Perot spectrometer for daytime airglow studies. *Journal of Atmospheric and Terrestrial Physics* 42, 499–511.
- Conde, M., Greet, P., Jacka, F., 1992. The Ring effect in the sodium D₂ Fraunhofer line of day skylight over Mawson Antarctica. *Journal of Geophysical Research* 97, 11,561–11,565.
- Fish, D.J., Jones, R.L., 1995. Rotational Raman scattering and the Ring effect in the zenith-sky spectra. *Geophysical Research Letters* 22, 811–814.
- Grainger, J.F., Ring, J., 1962. Anomalous Fraunhofer line profiles. *Nature* 193, 762.
- Greet, P., Conde, M., Jacka, F., 1989. Daytime observation of sodium layer with a Fabry–Perot spectrometer at Mawson. *Journal of Geophysical Research* 16, 871–874.
- Hays, P.B., Rusch, D.W., Roble, R.G., Walker, J.C.G., 1978. The O I (6300 Å) airglow. *Reviews of Geophysics* 16, 225–232.
- Narayanan, R., Desai, J.N., Modi, N.K., Raghavarao, R., Sridharan, R., 1989. Dayglow photometry: a new approach. *Applied Optics* 28, 2138–2142.
- Noxon, J., Goody, R., 1962. Observations of day airglow emissions. *Journal of Atmospheric Science* 19, 342–343.
- Pallam Raju, D., Sridharan, R., Gurubaran, S., Raghavarao, R., 1996. First results from ground-based daytime optical investigation of the development of the equatorial ionization anomaly. *Annales Geophysicae* 14, 238–245.
- Pallamraju, D., Baumgardner, J., Chakrabarti, S., 2000. A multiwavelength investigation of the Ring effect in the day sky spectrum. *Geophysical Research Letters* 27, 1875–1878.
- Pallamraju, D., Baumgardner, J., Chakrabarti, S., Pedersen, T.R., 2001. Simultaneous ground-based observations of an auroral arc in daytime/twilighttime O I 630.0 nm emission and by Incoherent Scatter Radar. *Journal of Geophysical Research* 106, 5543–5549.
- Rees, D., Conde, M., Steen, A., Brandstrom, U., 2000. The first daytime ground-based optical image of the aurora. *Geophysical Research Letters* 27, 313–316.
- Roble, R.G., 1995. Energetics of the mesosphere and thermosphere. In: Johnson, R.M., Killeen, T.L. (Eds.), *The upper mesosphere and lower thermosphere: a review of experiment and theory*. *Geophysical Monograph* 87, 1–21.
- Shepherd, G.G., Thullier, G., Gault, W.A., Solheim, B.H., Hersom, C., Alunni, M.J., Brun, J.-F., Brune, S., Charlot, P., Cogger, L.L., Desaulniers, D.-L., Evans, W.F.J., Gattinger, R.L., Girod, F., Harvie, D., Hum, R.H., Kendall, D.J.W., Llewellyn, E.J., Lowe, R.P., Oht, J., Peillet, F., Powell, I., Rochon, Y., Ward, W.E., Wiens, R.H., Wimperis, J., 1993. WINDII, the wind imaging interferometer on the Upper Atmosphere Research Satellite. *Journal of Geophysical Research* 98, 10 725–10 750.
- Solomon, S.C., Abreu, V., 1989. The 630 nm Dayglow. *Journal of Geophysical Research* 94, 6817–6824.
- Sridharan, R., Narayanan, R., Modi, N.K., Pallam Raju, D., 1993. A novel mask design for multiwavelength dayglow photometry. *Applied Optics* 32, 4178–4180.
- Sridharan, R., Modi, N.K., Pallam Raju, D., Narayanan, R., Pant, T.K., Taori, A., Chakrabarty, D., 1998. A Multiwavelength daytime photometer—a new tool for the investigation of atmospheric processes. *Measurement Science and Technology* 9, 585–591.
- Swift, W.R., Torr, D.G., Torr, M.R., Hamilton, C., Dougani, H., Richards, P.G., Sivjee, G.G., 1990. A procedure for the extraction of airglow features in the presence of strong background radiation. *Journal of Geophysical Research* 95, 15,227–15,241.
- Tepley, C.A., Meriwether, J.A., Walker, J.C.G., Mathews, J.D., 1981. Observations of neutral iron emission in twilight spectra. *Journal of Geophysical Research* 86, 4831–4835.